RESEARCH PAPER (BLUE)

Energy management strategy and capacity planning of an autonomous microgrid: Performance comparison of metaheuristic optimization searching techniques

Abba Lawan Bukar [a,b], Chee Wei Tan [a], Dalila Mat Said [a], Abdulhakeem Mohammed Dobi [a,c], Razman Ayop [a], Abdulgader Alsharif [a]

[a] Division of Electrical Power Engineering, School of Electrical Engineering, Faculty of Engineering, Universiti 5 Teknologi Malaysia, UTM, 81310 Skudai, Johor, Malaysia
[b] Department of Electrical and Electronic Engineering, Faculty of Engineering, University of Maidguri, P.M.B 1069, Maiduguri, Borno State, Nigeria
[c] Department of Electrical Engineering, College of Engineering, Waziri Umaru Federal Polytechnic, P.M.B. 10 1034, Birnin Kebbi, Nigeria

Electricity generation using renewable energy-based microgrid (REM) is a prerequisite to achieve one of the objectives of sustainable development goal (SDG 7- Affordable and Clean Energy). Nonetheless, the optimum design of the REM is challenging due to fluctuating demand and intermittent nature of the renewable energy sources. The optimum sizing of the REM is also associated with several non-convexities and nonlinearities, thereby precluding the application of deterministic optimization searching techniques for the sizing problem. This paper, therefore, proposes a rule-based algorithm and metaheuristic optimization searching technique (MOST) for the energy management (EM) and sizing of an autonomous microgrid, respectively. The purpose of the energy management scheme (EMS) is to provide power delivery sequence for the different components that compose the microgrid. Afterward, the EMS is optimized using MOST. For benchmarking, the paper compares the success of six different MOSTs. The simulation is performed for the climatic conditions of Maiduguri, Nigeria. The comparative results indicate that grasshopper optimization algorithm yields a better result relative to other studied MOSTs. Remarkably, it outperforms the grey wolf optimizer, the ant lion optimizer, and the particle swarm optimization by 3.0 percent, 5.8 percent, and 3.6 percent (equivalent to a cost savings of $8332.38, $4219.87, and $5144.64 from the target microgrid project). Results also indicate that the EMS adopted for the control of the microgrid has led to the implementation of a clean and affordable energy system. Moreover, the proposed microgrid configuration has minimized CO_2 emission (by 92.3 %) and fuel consumption (by 92.4 %), when compared to the application of a fossil fuel-based diesel generator.

Keywords: Metaheuristic algorithms; PV; Optimal sizing; Wind turbine; CO_2 emission

Introduction

Renewable energy technologies have been recommended as an intervention to alleviate the difficulties related to centralized electricity generation. This difficulties includes: extensive land use (for power transmission), high emissions (for a fossil fuel-based power generation), harmful waste generation (for a nuclear-based power), high power losses, excessive water use (for thermal-based power plant), and involve high investment

 https://doi.org/10.1016/j.ref.2021.11.004

Nomenclature

Symbol

σ	BT self-discharge rate (%/hour)
η_B	BT efficiency (%)
η_{inv}	Efficiency of inverter (%)
η_{pv}	Efficiency of PV (%)
η_{WT}	Efficiency of WT (%)
B_{cap}	BT bank capacity (kWh)
C_{BT}	Cost of BT ($)
$C_{BT,M}$	BT bank maintenance cost ($)
$C_{BT,R}$	BT replacement cost ($)
$C_{D_{GEN}}$	Cost of diesel generator ($)
$C_{GEN,M}$	Diesel generator maintenance cost ($)
$C_{D_{GEN,R}}$	Diesel generator replacement cost ($)
C_{inv}	Cost of inverter ($)
C_{PV}	Cost of PV module ($)
D_{GEN}	Diesel generator
H_2	Hydrogen
N_{PV}	Number of PV module
N_{WT}	Number of WT
n'_{BT}	BT lifespan (Year)
n'_{DEN}	Diesel generator lifespan (Year)

Abbreviations

ALO	Ant lion optimization
BT	Battery
CEMS	Circle-charging energy management scheme
COE	Cost of electricity ($)
CSA	Cuckoo search algorithm
DOE	Department of energy
DOST	Deterministic optimization searching techniques
DFA	Dragonfly algorithm
DPSP	Deficiency of power supply probability (%)
EM	Energy management
FC	Fuel cell
GA	Genetic algorithm
GA-PSO	Genetic algorithm-particle swarm optimization
GOA	Grasshopper optimization algorithm
GWO	Grey wolf optimization
HGWOSCA	hybrid GWO-sine cosine algorithm
HSA	Harmony search algorithm
IHSA	Improve harmony search algorithm
MOV	multi-verse optimizer
NFL	No-free lunch
NPC	Net present cost ($)
n'_{inv}	Inverter lifespan (Year)
n_{WT}	WT turbine lifespan (Year)
T^{noct}	Nominal operating temperature (^oC)
n'_{PV}	PV module lifespan (Year)
$C_{PV,M}$	PV maintenance cost ($)
C_{WT}	Cost of WT ($)
$C_{WT,M}$	WT maintenance cost ($)
DoD	Depth of discharge (%)
d'	Nominal interest rate (%)
n'_{WT}	WT lifespan (Year)
P_l	Energy demand (Watt)
P_r^{PV}	PV module rated power at standard test condition (Watt)
P_r^{wt}	WT rated power (Watt)
P_r^{DG}	Diesel generator rated power (Watt)
V_b	BT voltage (Volt)
V_s	System voltage (Volt)
V_{in}	Cut-in speed (m/s)
V_{out}	Cut-out speed (m/s)
V_R	Wind turbine rated speed (m/s)
f	Inflation rate (%)
PV	Photovoltaic
SCA	Sine cosine algorithm
SOC	State of charge
SSO	Social spider optimizer
SSA	Salp swarm algorithm
REM	Renewable energy based microgrid
RES	Renewable energy source
WT	Wind turbine
SA	Simulated annealing

cost [1,2]. Nonetheless, the sporadic behaviour of renewable energy sources (RESs) affects the electricity supply and incurred additional costs on electricity consumers and the electricity utility company. Thus, this has affected tremendously the deployment of the RESs specifically for the off-grid usage [3]. As such, the development of a smart microgrid is a potential approach to allow the RESs to be incorporated into a microgrid. According to the United State Department of Energy (DOE), a microgrid is defined as *"a cluster of interconnected distributed energy resources and loads within clearly defined electrical boundaries that acts as a single controllable entity with respect to both islanded-mode or grid-connected network."* In spite of this definition; it is generally accepted in the research community that this description can also be applied to the case of an off-grid microgrid which has no connection to large-scale upstream grid-network [4].

Microgrid capacity planning background: Problem characteristics and research gap

Microgrid capacity planning belong to a combinational class of optimization problems. This class of optimization problem is a multi-modal, multi-variable, multi-objective and is characterized by various sources of nonlinearities, constraints and non-convexities [5–8]. The methods used to resolve this class of optimization problem are affected by high overheads during the computation procedures. Over the last two decades, finding a realistic approach to accurately compute for the capacities of the microgrid elements has been the focus of the microgrid designers.

As such, various optimization methods have been reported in the literature for resolving the capacity problem of microgrid. This includes, deterministic optimization searching techniques (DOSTs) and metaheuristic optimization searching techniques (MOST) [9–11]. The DOSTs have poor local search ability; follow rigorous protocols, prone to stagnation in the local optima and inflexible to trace the changes in the in the optimization fitness function [5]. Thus, the DOSTs are rarely used nowadays for the microgrid optimization problems. In recent time, the MOSTs are often applied to compute for a variety of renewable energy (RE) systems (nano-grids, virtual power plants, microgrids *e.t.c*) design and capacity planning problems, which can be viewed as a power engineering optimization problems [12]. The MOSTs alleviate the limitations associated with the DOSTs and are very

easy to execute [13,14]. Even though not all the MOSTs guarantee global optimum, their dominance over the DOSTs has been verified in the microgrid planning research [9].

As an example, Malaki *et al.* [15] have proposed an improve harmony search algorithm (IHSA) to calculate the capacity of a hybrid photovoltaic (PV)/battery (BT) storage unit. The objective of the optimization to determine the optimum capacity of the hybrid system, require to supply the electricity demand of a remote homes in Iran at minimum life cycle cost (LCC). The author concluded that the application of the IHSA offers a more promising result compared simulated annealing (SA) and harmony search algorithm (HSA). Li *et al.* [16] have devised a microgrid sizing method using genetic algorithm (GA). The microgrid incorporate a solar heating system/PV modules/air conditioner/heat boiler-/hydrogen (H_2) based back-up system/BT/heat chiller/a heat storage system, serving as a cooling, thermal, electrical, and H_2 load demand of an isolated area. Mohseni *et al.* [17] have devised a month flame optimization algorithm (MFOA) to minimize the net-present cost (NPC) of a grid-independent microgrid and used equivalent loss factor to evaluate the reliability of the microgrid. The sizing results computed by the MFOA is compared with the results found by GA, GA-PSO and PSO. In [18], optimal sizing for a hybrid grid- independent microgrid have been designed using sine-cosine algorithm. The optimization aims to minimize the whole LCC the hybrid energy system considering the loss of load interruption probability (LLP) as reliability in index. Fathy [19] have applied social spider optimizer (SSO) to optimally size a hybrid wind (WT)/BT/PV/diesel generator (D_{GEN}) integrated microgrid and have shown its supremacy over ALO, whale optimization algorithm, GWO, multi-verse optimizer (MVO), harris hawks optimizer (HHO). Nasiraghdam *et al.* [20] have employed the artificial bee colony optimization method (ABC) to optimize the capacity of wind turbine (WT)/-fuel cell (FC)/PV microgrid system and have demonstrated its superiority over PSO and GA methods. Chauhan and Saini [21] have applied discrete HSA for the optimal planning of an off-grid microgrid incorporating a biomass gasifier/biogas digester system/WTs/PVs/micro-hydro plant (MHPP).

In addition to the above studies, recently the application hybrid algorithm has also been reported in the literature. For example, Mohandas *et al.* [22] have integrated artificial bee colony (ABC) and chaotic theory optimization method and used it for the design of distributed generation units. The authors have affirmed the superiority of the devised hybrid method over the basic ABC algorithm. In [23], Jahannoosh *et al.* have used a hybrid GWO-sine cosine algorithm (HGWOSCA) to design a cost-effective renewable energy system comprising of PV/FC/WT to supply the residential demand of a commercial centre situated in Iran. The authors have demonstrated the superiority of the proposed HGWOSCA algorithm over PSO, GWO, and SCA. Jiao *et al.* [24] have upgraded the standard harmony search algorithm (HSA) by expanding its search space range and enhanced the interaction between the global and local procedures. The modified HSA is applied to solve the sizing problem of a standalone microgrid, and its outperformance have been confirmed when it is benchmarked with PSO technique and classic HSA. Derakhshan *et al.* [25] have enhanced the performance of the classic cuckoo search algorithm by accommodating crossover operators and using it to optimize the parameters of a grid-connected WT-BT-PV microgrid. Despite the hybridization of the metaheuristic optimization algorithms, a major problem of making such inferences in the classification of the preceding works is that there is no insight as to why those MOSTs are chosen to be improved. Hence, this is a thoughtful criticism of all the previous works that belong into this classification. Likewise, since PSO and GA are the widely and well-documented techniques in this field of research, they are usually applied as references methods to investigate the efficiency of other MOSTs [9]. A detailed overview and comparison of the MOSTs employed for microgrid capacity planning can be found in [5,13,26].

Objectives and contributions to the study

Although various MOSTs have been recommended for computing microgrid capacity planning problem, however, owing to the stochastic nature of the MOSTs, there is still need for a continuous examination of the efficiencies of newly developed MOSTs, whose potential advantages have not yet been investigated in this field of research [5]. This is essential because a minor improvement in the MOSTs will positively affect the cost of the microgrid and the capacities of its elements. Moreover, the reason why newly developed MOSTs could outperform those that have been earlier used in the microgrid planning analysis lies in the so-called no-free lunch (NFL) theorem [10] and the ever-evolving nature of the MOSTs. The theorem has logically proven the inability to generalize the performance of MOST for a particular problem across different disciplines and research areas. This, however, creates the possibility to put forward newly emerge MOSTs and estimate their performance in resolving diversified polynomial-time hard problems.

In this light, this paper attempt to investigate the efficiency of six MOSTs for the capacity planning problem of an autonomous hybrid energy system. The proposed system is intended to supply the electricity demand of off-grid residences in Nigeria. The following recently developed MOSTs are considered in this comparative study: (i) grey wolf optimization (GWO) [27] (ii) dragonfly algorithm (DFA) [28], (iii) cuckoo search algorithm (CSA) [29], (iv) the grasshopper optimization algorithm (GOA) [30], (v) salp swarm algorithm (SSA) [31], (vi) ant lion optimization (ALO) [32]. In addition, one of the most widely and well-known MOSTs used for microgrid capacity planning, *i.e.* PSO [33], is also embedded in the capacity planning method separately. Afterward, the efficiencies of the aforementioned MOSTs are compared based on the quality of solutions and convergence. It should be remembered that in this study, PSO is considered as the reference method, because its performance is acknowledged and widely accepted in literature.

On the other hand, based on the review conducted on microgrid capacity planning, it indicates that energy management scheme (EMS) is not modelled and incorporated in the microgrid capacity planning phase [6,15,18,25,34–36]. This is however, a drawback, because, without a proper EMS, the computed microgrid capacity might rise to reliability issue which in practice is key in ensuring the resilient operation of the microgrid. Based on the foregoing drawbacks, this paper incorporates a cycle-charging EMS (CEMS) during the capacity planning phase of the microgrid. The rule-algorithm is selected for the implementa-

tion of the CEMS because it provide exact solution, computationally efficient and efficient for real-time application [37].

The core contributions of this paper are outlined as follows:

1. Modeling of simulation prototype for an autonomous WT-PV-diesel generator (D_{GEN})-BT microgrid which serves as a practical microgrid to examine the applicability of the planned microgrid capacity planning approach.
2. Based on the simulation prototype modeled in (1) a control strategy CEMS is developed for the microgrid using a rule-based algorithm. The CEMS coordinates and provide power delivery sequence for the different energy sources in the microgrid.
3. A universally bio-inspired MOST is devised for optimum sizing of the autonomous microgrid, and the efficiencies of six recently developed MOSTs are investigated. The outcomes of the MOSTs are compared statistically with the outcome realized by a well-documented and widely MOST used for microgrid capacity planning.
4. A comprehensive analysis of the cumulative revenue generation incurred from the microgrid and the discounted break-even analysis is performed, which, in turn, indicates the dynamic payback period of the microgrid.
5. Direct comparison of the CO_2 emission and fuel consumption between the proposed microgrid energy system which adopts CEMS as its control strategy and conventional D_{GEN}.

The rest of the paper is structured as follows. Section 2 presents the microgrid prototype employed as a test-case system to demonstrate the applicability of the microgrid capacity method and which serves as a platform for the comparison of the performances of the selected MOSTs, as well as the CEMS used for the control and operation the microgrid. In section 3, the control strategy (EMS) employed for the operation of the microgrid is elaborated. Section 4 presents the application of the applied MOSTs to optimize the microgrid and problem formulation is stated. Section 5 highlights the modelling framework for the autonomous microgrid, this is followed by the results and discussion of the study in Section 6. The conclusions, drawbacks of the research, and area for future research are outline in Section 7 and Section 8, respectively.

Schematic of the autonomous microgrid

The structure and energy flow of the autonomous microgrid is presented in Fig. 1. The green and blue lines in the figure represent communication/control and communication only power lines. The dotted arrows signify the electricity power lines. The conceptualized microgrid test-case system is composed of a diesel generator (D_{GEN}), PV panels, WT, battery (BT), a converter, and a dump load (irrigation system). The mathematical model of the microgrid test-case system components and as well the technical and economic parameter of the components depicted in Table 1 is according to Ref. [38].

Proposed microgrid control strategy

The intermittent behaviour associated with RE sources is the reason why the energy management scheme (EMS) has become very challenging. Consequently, to design a reliable microgrid, single RE source cannot be relied upon to meet the demand. The reliability of the system can be enhanced by integrating RE sources and energy storage system as primary backup source to keep a balance between the generation and the demand. The system operator must ensure that the RESs are used first to reduce the electricity cost and optimize the operation of the storage medium (maintain depth of discharge (DoD), SOC maximum, SOC minimum). This can only be realized using strategic and robust EMS. The EMS aims to manage the operating sequences of the elements in the microgrid, provide a power delivery sequence for the subsystem that composed the microgrid, minimize BT degradation, and minimize CO_2 emission [39,40].

The microgrid capacity planning method proposed in this study adopts CEMS as the microgrid operational strategy. The CEMS operational strategy is developed using a rule-based algorithm. The rule-based method is primarily in the form of 'if-then' descriptions. The "if", statements are associated with different scenarios and 'then' statement executes the operating modes. A comprehensive note on the ruled-based algorithm can be found in Ref. [37,41]. In this study, the operation scenarios are defined based on the values of the minimum and maximum state of charge (SOC) of the BT, load demand (P_l), the WT power ($P_{WT}(t)$), and PV power ($P_{pv}(t)$). Subsequently, the rule-based algorithm decides on the subsystem to turn OFF/ON. Hence, five modes of operation are considered for the operation of the autonomous microgrid. The microgrid modes of operation are described in the following subsections.

Operating mode 1: Photovoltaic and wind power supplying demand

The transfer of energy from PV array and WT to P_l is carried out using this operating mode, *i.e.,* $(P_{pv}(t) + P_{WT}(t))$ power to supply P_l. Priority is given to PV and WT to fulfill demand since they are considered as the main power source. This operating mode is depicted in Fig. 2a.

Operating mode 2: Photovoltaic and wind power supplying demand and battery charging

This operating mode is responsible for charging of the BT bank. When $P_{PV}(t)$ and $P_{WT}(t)$ is sufficient to fulfill P_l and then extra power that cannot be absorbed by the P_l will be channeled to the BT bank. This operating strategy is illustrated in Fig. 2b.

Operating mode 3: Photovoltaic and wind power supplying demand and dump load

This operating mode allows the E_{dump} to be energized. When the sum of $P_{pv}(t)$ and $P_{WT}(t)$ is greater than the $P_l(t)$, and BT bank $SOC(t) = \overline{SOC}$, the extra power that cannot be absorbed by the BT bank and P_l will used to supply the dump load (such as irrigation system). This operating is mode is depicted in Fig. 2c.

Operating mode 4: Photovoltaic, wind power and battery supplying demand

In this operating mode, if $P_{pv}(t) + P_{WT}(t) < P_l(t)$, then the energy absorbed by the BT bank in operating mode 2 is allowed to discharge. However, BT is allowed to discharge up to its minimum

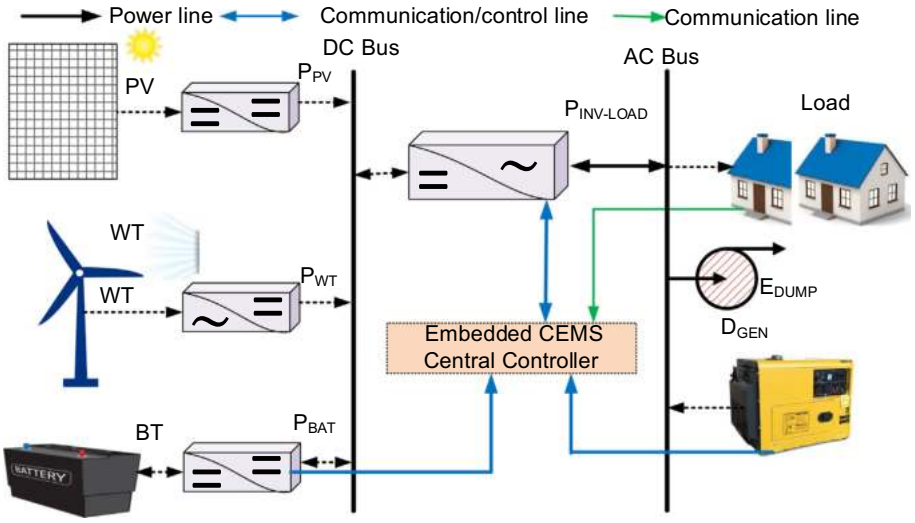

FIG. 1

The architecture of the proposed autonomous microgrid.

allowable SOC set point. This operating is mode is depicted in Fig. 2d.

Operating mode 5: Diesel generator supplying demand and battery charging

This operating mode allows the usage of the D_{GEN}. In this mode, D_{GEN} is turn ON to charge BT bank and supply $P_{l,}$ for as long as $P_{pv}(t) + P_{WT}(t) < P_l(t)$ and BT $SOC(t) < \underline{SOC}$. The D_{GEN} is switched OFF when $P_{pv}(t) + P_{WT}(t) \geq P_l(t)$. This operating is mode is depicted in Fig. 2e. The overall algometric flowchart of the CEMS is presented in Fig. 3.

The metaheuristic-based optimal capacity planning method

This section outlines the formulation of the MOST-based method for determining the optimal capacity of the considered autonomous of the microgrid components. The devised method minimizes the cost of electricity (COE) and the deficiency of power supply probability (DPSP) of the microgrid as the optimization criterion, to estimate the number or the size of elements in the microgrid, subject operational and reliability constraints. The fitness function is then minimized iteratively by applying the aforesaid seven MOSTs to compute for the optimal capacities of the microgrid elements. The microgrid is then tested according to the determine capacities at each iteration, to confirm whether the reliability and operational limits imposed on the microgrid is met. Lastly, the optimum capacity combination of the elements at the last iteration count (the best solution set), which has the lowest COE, is reported.

All the examined MOSTs begin by generating a matrix of random particles or individuals. The particles, then evolve towards the optimum (solution) in the search-landscape, using their fitness function values as the estimation criterion. The stirring (evolution) procedure towards the optimum solutions is set continuously according to the different operators and rules specified for each of the MOSTs until the stopping criterion (i.e., the maximum number of iterations) is reached. Detail description of the employed MOSTs can be found in [27–32].

Fitness function

Based on the above discussion, the minimization of the COE generation of the considered microgrid project, and at the same time satisfying the electricity requirement of the demand, a methodology is devised in this section. The fitness function (COE) is derived from the life cycle costs of the microgrid using the total net-present cost (TNPC) concept. The TNPC of the encompasses the summation of the NPCs of the microgrid elements. It can be defined as [42,43]:

$$NPC_T = NPC_{BT} + NPC_{WT} + NPC_{PV} + NPC_{CON} + NPC_{D_{GEN}} \quad (1)$$

where $NPC_{BT,}NPC_{WT,}NPC_{PV,}NPC_{inv}$, and $NPC_{D_{GEN}}$, respectively represents the NPCs of the BT bank, WT, PV panels, inverter and the D_{GEN}, each of which can be determined by Eq. (2) [5].

$$NPC = N.(CC + RC \times K + O\&M \times \frac{1}{CPV(d,R)} \quad (2)$$

where N denotes the optimum (number/capacity) of the element; O&M, RC and CC denote the operation and maintenance costs, replacement cost and capital cost respectively. K and CRF, respectively stand for the one-time payment for the present worth and capital recovery factor. The CRF can be calculated using Eqs. (3) and (4) [42].

$$CRF(i,R) = \frac{(i+1)^l}{(i+1)^l - 1} \quad (3)$$

where i stands for the interest rate per annum, it can be determined using Eq. (4). l stands for the project life-time of the microgrid and is considered to be 25 years (in compliance with the lifespan of the PV modules as the most durable element of the system.

$$i = \frac{d^{'} - f}{1 + f} \quad (4)$$

where f represent the inflation rate and $d^{'}$ is the nominal interest rate (i.e the interest rate at which money is borrowed from the

TABLE 1

Technical and economic specification of the microgrid components.

Parameters	Values	Unit
Photovoltaic		
n'_{PV}	25	years
C_{PV}	2.15	$/$W_p$
P_r^{pv} at STC	275	W
T^{noct}	45±2	°C
T^{cof}	-3.4×10^{-3}	1/°C
η_{pv}	16.9	%
$C_{PV,M}$	20	$/year
Regulator cost	1500	$
Wind turbine		
n'_{WT}	25	years
P_r^{wt}	1	kW
V_R	9.5	m/s
V_{in}	2.5	m/s
Regulator cost	1000	$
$C_{WT,M}$	50	$/year
C_{WT}	3	$/W
V_{out}	20	m/s
η_{WT}	92	%
Battery		
n'_{BT}	2	years
C_{BT}	280	$/kWh
$C_{BT,M}$	5	$/%
B_{cap}	45.2	kWh
Σ	0.007	%/hour
DoD	70	%
$C_{BT,R}$	280	$/kWh
SOC maximum	100	%
SOC minimum	30	%
V_b	12	V
V_s	48	V
η_B	0.85	%
$B_{cap(single)}$	250	Ah
Diesel generator		
$C_{D_{gen}}$	1000	$/kWh
P_r^{DG}	4	kW
n'_{DEN}	24000	Hours (5years)
$C_{D_{gen,R}}$	1000	$/kWh
$C_{gen,M}$	0.064	$/h
S_f	0.689	$/L
Economic Parameter		
d'	12	%
Project n′	25	Year
f	4	%
Inverter		
n'_{inv}	15	Years
η_{inv}	92	%
C_{CON}	2500	$

bank for the project). Currently, the inflation and nominal interest in Nigeria are 4% and 12% (The values are computed by taking the average of the rates obtained from various banks in the Nigeria) [44].

As stated previously, the reliability indicator of the microgrid is assessed using the concept of DPSP. It can be measured using Eq. (5), and must be 0% [5].

$$DPSP = 100.\frac{\sum_{i=1}^{N} hours[P_{supp}(i) < P_{dem}(i)]}{N} \quad (5)$$

where P_{supp} and P_{dem} respectively, represent the supplied electrical energy and energy demand. N represents the total number of hours. A $DPSP = 0\%$ means electricity demand will be fulfilled at all times. $DPSP = 1\%$ is an indication that consumer demand will not be met. In this study, a DPSP of zero is considered for the analysis. The fitness function is to be minimized using the seven MOSTs. The MOSTs are incorporated with the CEMS to optimize the microgrid. The PSO being the famous optimization algorithm is adopted to test and confirm the effectiveness of GWO, DA, CSA, GOA, ALO, SSA.

Constraints

The optimization of the fitness function is subject to restrictions on the operation of components. In general, the optimization problem is formulated with three constraints: (1) the one associated with the reliability to ensure the steadiness of electricity supply, refer to Eq (5); (2) those associated with the equality of the final and initial energy content of the BT bank (SOC minimum and maximum), and (3) the constraint associated to the lower and upper boundaries of the non-negative design variables which are as follows:

$$20 \le N_{PV} \le 45; 0 \le N_{WT} \le 10; 0 \le N_{AD} \le 3 \quad (6)$$

Summary of the modelling framework for the autonomous microgrid

The summary of the computational frame for the design of the autonomous microgrid is depicted in Fig. 4. This modeling framework is used to optimize the design of the autonomous microgrid (by minimizing the fitness functions mentioned above and at the same time adhering to the constraints imposed), thereby assessing the efficiencies of the MOSTs. The load profile imposed on the microgrid and climatological data of the case study region, the economic and technical parameters of the microgrid components, product model, operating mode of the CEMS; as well as the interest rate and the project life-span are used as input to the model. This is followed by implementing the CEMS program and incorporating it into the MOSTs. The fitness function is minimized iteratively to compute for the optimum capacities of the design variables. The microgrid system is tested using the values computed for the design variables. Lastly, the computed capacities of the components are chosen as the optimum capacities.

Results and discussion

The grid-independent microgrid depicted in Fig. 1, is applied to investigate and confirm the devised microgrid capacity planning method by investigating the impact of the applied MOSTs on the COE of the microgrid, and the rate of convergence. The computational test was performed on Intel®, processor 3.20 GHz CPU, 8 GB RAM, Core ™ i7-8700. All models were coded and run-on MATLAB 2019a software.

Climatological and energy demand data

A case study region was chosen to test the applicability of the devised microgrid EMS and capacity planning approach proposed in this paper. The microgrid is intended to supply the electricity demand of residences in an isolated community in Yobe

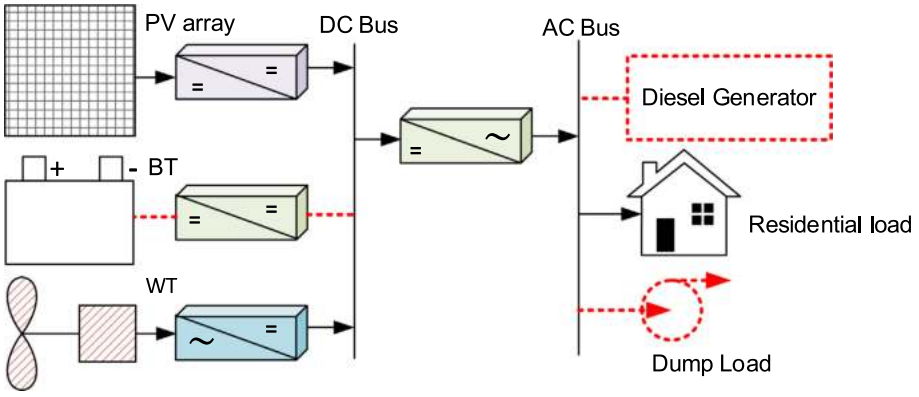

FIG. 2A

Photovoltaic and wind power supplying demand.

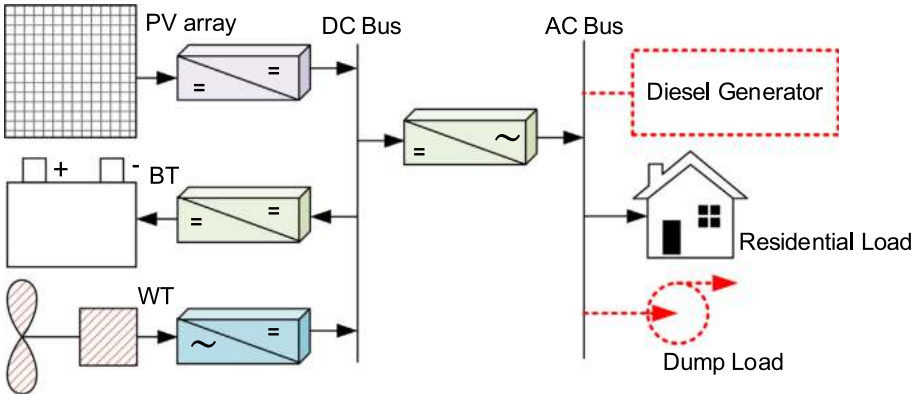

FIG. 2B

Photovoltaic and wind power supplying demand and battery charging.

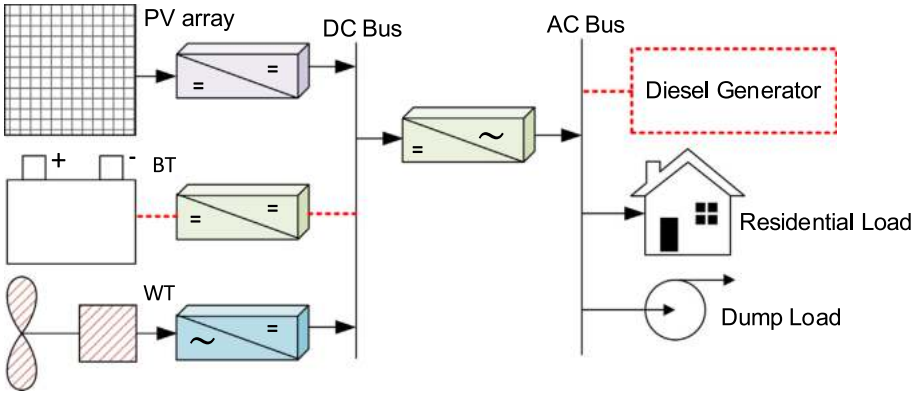

FIG. 2C

Photovoltaic and wind power supplying demand and dump load.

State, Nigeria whose Latitude and Longitude are 12.1871° N and 11.7068° E, respectively. The number of residences for which the microgrid is conceptually developed is five, with a population of about forty-five. The study region has good solar and wind resources with low season variations of electricity generation. Figs. 5–7 depicts the hourly ambient temperature, the hourly wind speed (measured at 10 m) and the hourly solar irradiance with their corresponding contour map for a period of one-year. The climatological data were sourced from the Nigeria Meteorological Agency (NIMET) database [45]. While the residential load profile imposed on the microgrid is given in Fig. 8. The load profile data was sourced from a survey conducted by the Power Holding Company of Nigeria (PHCN) for the energy consumption pattern in remote residence.

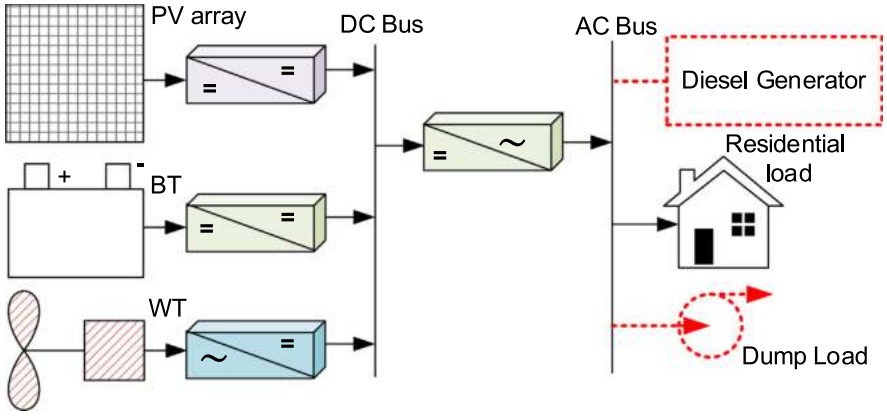

FIG. 2D

Photovoltaic, wind power and battery supplying demand supplying demand.

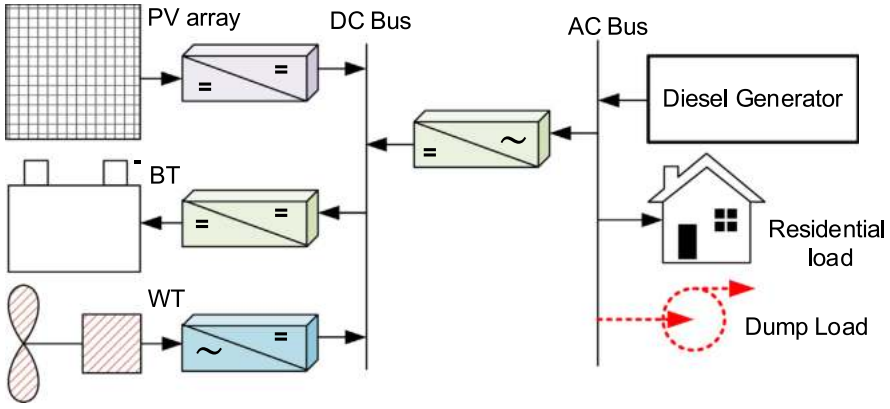

FIG. 2E

Diesel supplying demand battery charging.

Verification of the CEMS resiliency

This section demonstrates the performance of the CEMS operational strategy before optimizing it with the devised MOST's microgrid capacity planning approach. The verification of the rule-based CEMS is intended to study the resiliency of the rule-based algorithm and the operation of the scheme over a long period and to confirm that the BT bank operational limit is not violated despite the seasonal discrepancies on the output of the $P_{PV}(t)$ and P_{WT}. In this context, the BT bank's initial state of charge of the initial state of charge of the BT bank is set to 80% and its DoD is set to 70%. A WT rated 5 kW, PV array rated 5.8 kW, D_{GEN} rated 2 kW, and a 12V/250Ah BT, with a rated capacity of 45.2 kWh is used for the confirmation of the CEMS resiliency. Fig. 9 portrays the hourly simulation of the energy mix and the corresponding SOC of the BT, for 1-year operational time frame. Moreover, for clarity purpose, Figs. 10–12, illustrates the electricity mix of the microgrid (on the left-ordinate) and the corresponding BT bank SOC (right-ordinate) during the rainy, cold, and hot season respectively, for 2-day operational time frame.

It can be noticed from the figure (Fig. 10) that the rise and fall of the P_{PV} during day during the cold season is reasonably smooth. Hence, this indicate a normal weather condition and the solar irradiance is not disturbed by the weather condition. During hour 1 h to 9 h, the P_{PV} and P_{WT} is not insufficient to meet P_l by operating Mode 1 (P_{PV} and P_{WT} to supply P_l). In this situation, the P_l is fulfilled by activating operating Mode 4 (P_{PV}, P_{WT}, and BT to supply P_l), thereby discharging the from the BT bank (BT_{dch}) to meet the P_l (this is denoted by the positive blue line of Fig. 10).

For clarity, the summary of the hour-by-hour operation of the CEMS during the cold, hot and rainy season is given in Tables 2–4. Regarding, the cold season, it can be noticed that, from the sunrise to sunset *i.e.* 9 h to 18 h, the P_{PV} and P_{WT} has exceed the P_l, as such operating Mode 2 (P_{PV} and P_{WT} to supply P_l and BT charging) is activated. This mode enables the P_l to be energies and the surplus power which cannot be absorbed by the P_l is used to charge the BT bank (BT_{ch}) (refer to the negative blue line of Fig. 10). Moreover from 18 h to 19 h, Mode 1 is activated because the P_{PV} and P_{WT} is sufficient to meet the P_l, however without any extra power. At 18 h to 33 h, the PV power is no longer available due to sunset, while the P_{WT} is insufficient to meet the P_l. Therefore, operating Mode 4 is activated to supply the P_l. Similarly, at 33 h to 41 h and 41 h to 48 h, Mode 3 and Mode 4 are executed to supply demand, respectively. It is worth mentioning that during the 48 h of operation time-frame, only Mode 2, Mode 1 and Mode 4 are executed. Furthermore, the minimum SOC attained by BT is

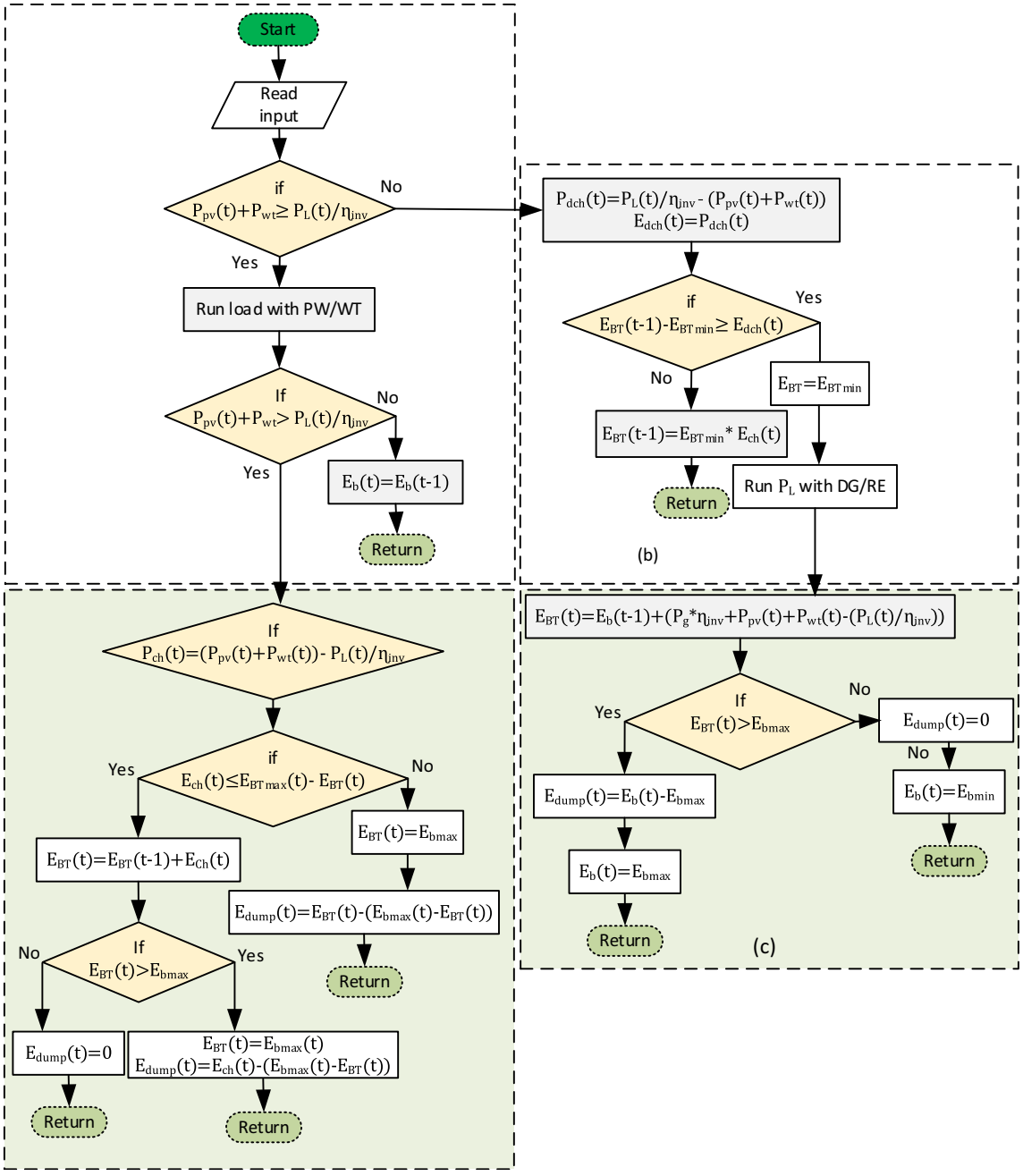

FIG. 3

Algorithmic flowchart of the rule-based CEMS, (a) The main CEMS flowchart algorithm (b) CEMS execution for BT bank to discharge (c) CEMS operation for D_{Gen} to switch ON and OFF (d) CEMS operation for BT bank to charge.

36.07% (17.4 kWh) and the maximum attained is 99.2% (44.74 kWh).

Performance comparison of the applied MOSTs for the microgrid capacity planning

To perform a fair comparison among the considered MOSTs, their particles/individual, and the maximum generation (iteration) for all the studied algorithms are kept constant (5 particles and 100 iterations are considered). The remaining parameters of the MOSTs examined are tuned according to the values suggested by their creators, which are given in Table 5 [27,28,30–33]. Note that the GWO and ALO do not need parameter tuning because their parameters are modified during iteration. Moreover, it is commonly demonstrated that 30 independent simulation runs are sufficient to compare the efficiency of different MOSTs [46]. For each of the MOSTs, therefore, the optimization program is run for 30 times. Subsequently, a statistical-driven method is then employed, to compares the efficiencies of the MOSTs, taking into account their effectiveness in computing for the optimal design capacity of the microgrid. The comparison method uses four statistical indicators: the mean outcome (mean), the median outcome (median), the worst-case outcome (worst), and the best-case outcome (best) of the COE, discovered for the microgrid model over the 30 independent simulations conducted. The

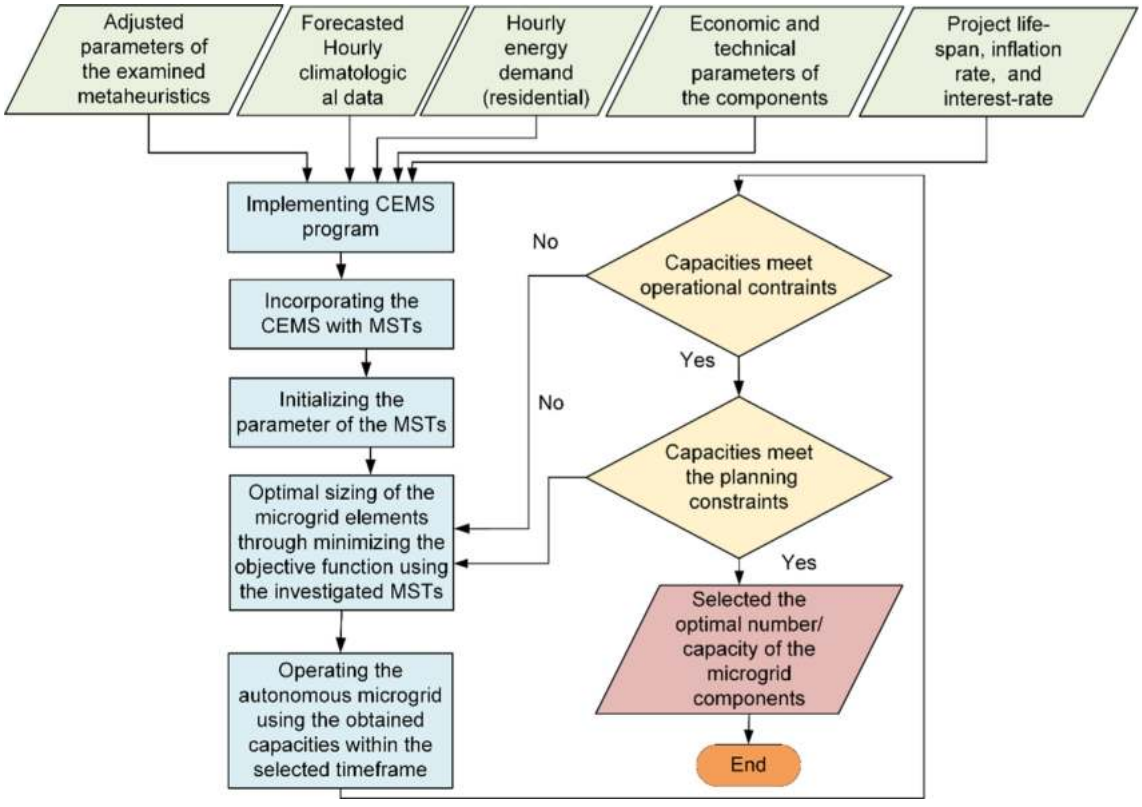

FIG. 4

Flowchart of the proposed CEMS MOST-based optimal capacity planning method.

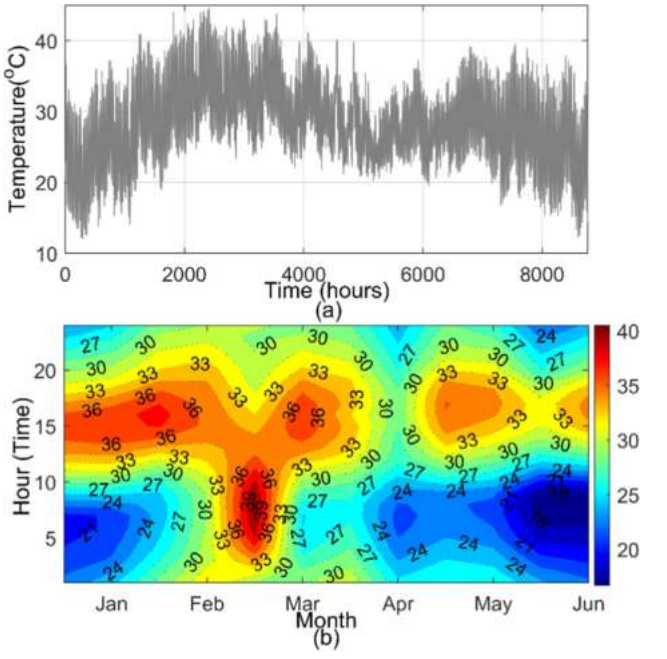

FIG. 5

(a) Hourly ambient temperature of the studied site (b) Contour diagram of the monthly-average ambient temperature (°C).

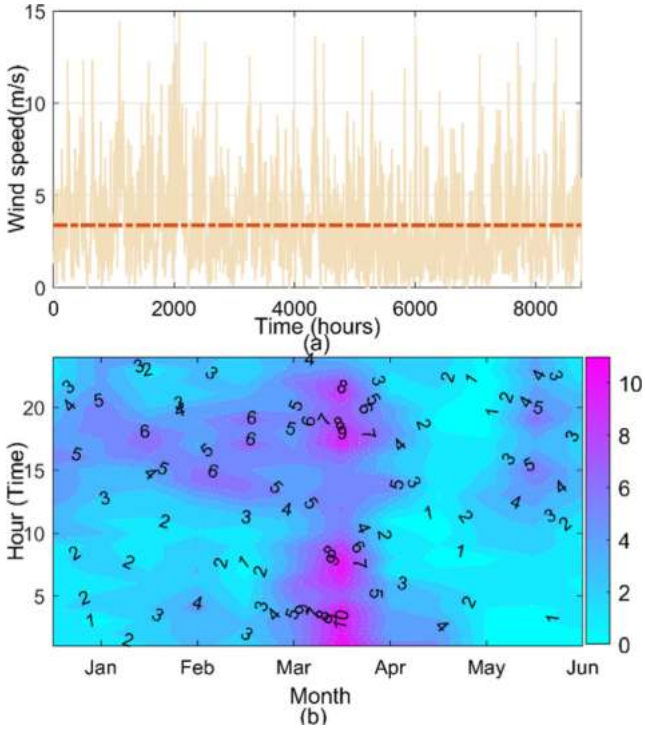

FIG. 6

(a) Wind velocity of the studied site and (b) Contour diagram of the monthly-average ambient temperature (°C).

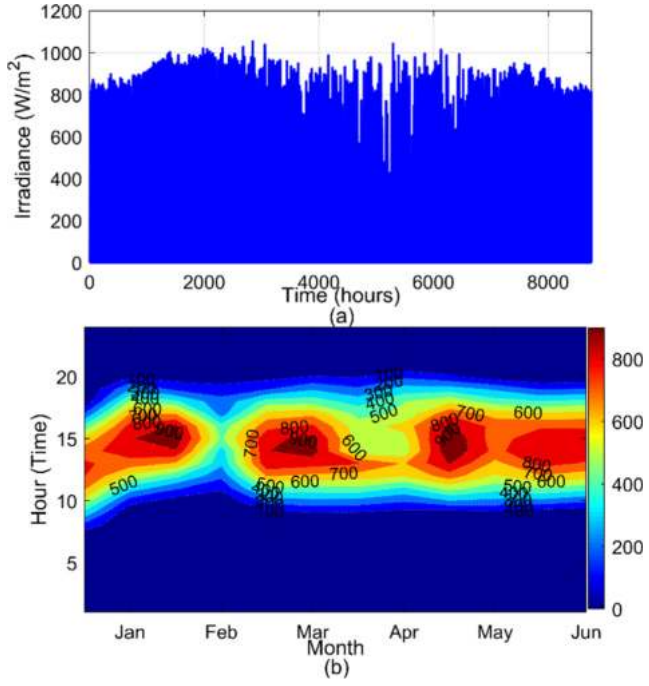

FIG. 7

(a) Hourly solar irradiance of the studied site (W/m^2) (b) Contour diagram of the monthly-average solar insolation (W/m^2).

worst, mean, and best metrics indicate the accuracy of the MOST. The median reflects the precisions of the MOST (*i.e.,* the number of successes out of 30 trials to the optimum solution). Table 6 ranks the performance of the MOSTs under investigation based on the aforementioned statistical framework.

In Table 6, it can be observed that CEMS-ALO and CEMS-GOA respectively demonstrate the worst and best results within the context of the devised method. These statistics-based outcomes give a convincing confirmation of the supremacy of the CEMS-GOA over CEMS-PSO and CEMS-CSA (which are well-known MOSTs) and even CEMS-ALO, CEMS-DFA, CEMS-GWO, and CEMS-SSA (which are most recent MOSTs in the literature). Based on the outcome of the results, the CEMS-GOA has result to a saving of 0.32% and 0.69% in the COE of the microgrid in comparison to CEMS-CSA and CEMS-GWO. It has also contributed to a saving of 0.78%, 0.96%, 1.61%, and 2.34%, respectively in the COE compared to CEMS-PSO, CEMS-SSA, CEMS-DFA, and CEMS-ALO. The supremacy of the CEMS-GOA stems from its fair exploitation and exploration capability during the search process. This is due to the updated procedures of the grasshoppers, in which the positions of the grasshopper are updated based on the feasibility and trajectory of the grasshopper, which enhances the search of the feasible design search space. Table 7 provides a detailed combination of the system constituent computed by the studied MOSTs for the best results obtained.

Fig. 13 depicts the convergence curves of the employed MOSTs for the trial, in which the methods showed their best results in terms of approaching the global optimum. Also indicated in subfigure Fig 13(a), the CEMS-PSO method has the highest convergence rate as compared to all the studied techniques tested and estimates the global optimum in the 6th iterations. The results in Fig. 13, also indicates that CEMS-GWO, which is ranked the third-best, has a convergence trend similar to CEMS-PSO in the early stages of iterations, however, converges slower at the later stage. The CEMS-GOA shows a strong ability to explore the design search space in the last iterations, while the other MOSTs are trapped in the local optimum point. Hence, this highlights the strong exploitation ability of the CEMS-GOA. Lastly, the CEMS-SSA, CEMS-DFA, and CEMS-ALO were not only stuck in the local optimum but also had the characteristics of poor convergence.

Breakdown of the TNPC

This section presents the breakdown of the TNPC of the microgrid over the operational timeframe of the microgrid. The analysis is performed using the results obtained for the CEMS-GOA, which has demonstrated high superiority among the studied

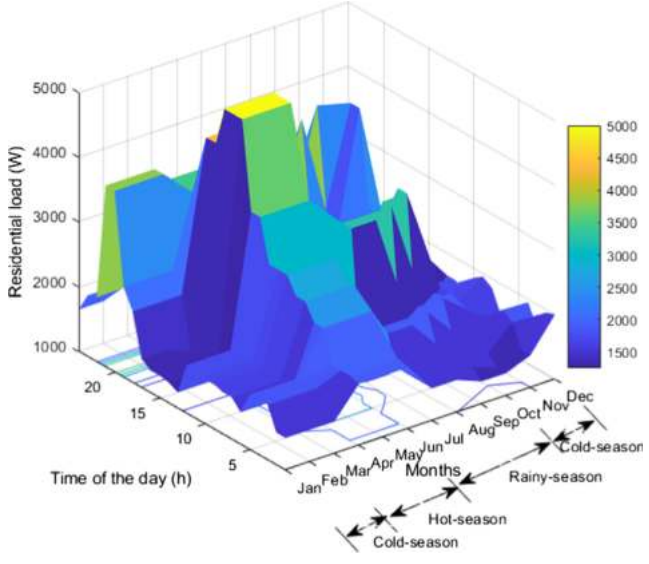

FIG. 8

3D diagram of the monthly average day-time discrepancies of residences load profile.

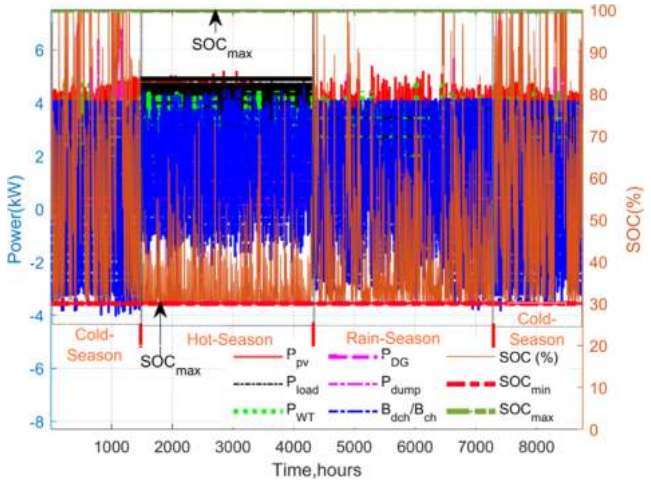

FIG. 9

CEMS results for a year-round operation.

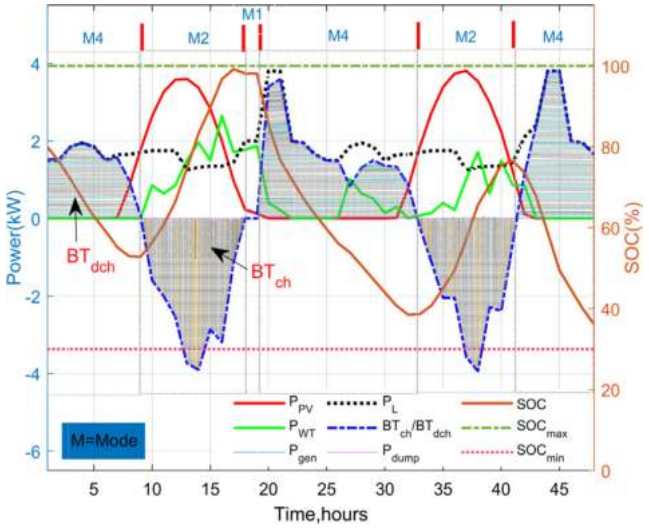

FIG. 10

Plot of electricity generation mix against the BT bank (cold-season).

MOSTs and having TNPC of $135,899.62. The O&M costs, replacement costs, and capital cost of the microgrid account for 33.96%, 17.17%, and 44.87% of the TNPC, respectively. Furthermore, it should be noted that this study does not account for the salvage value of the microgrid investment program. This is because we believed that the project will not be abandoned at the end of the payback period of the microgrid. Fig. 14 break down the TNPC of the microgrid elements. As demonstrated in the figure, the contribution of the WT, PV array, inverter, and BT bank to the TNPC amount to 10.81%, 13.18%, 3.8%, 38.51%, and 33.70%, respectively. The BT bank and D_{GEN} which serve as primary and secondary backup power supply occupies the largest proportion of the TNPC. Fig. 15 depicts the breakdown of the microgrid energy system cash flow for the case study area under consideration. As outlined in the figure, the replacement costs are incurred only by the D_{GEN}, BT bank, and the inverter. Moreover, all the elements in the microgrid incur O&M except the inverter. The D_{GEN} incur large portion of the O&M due to the fuel cost. It is also worth mentioning that the COE calculated using the CEMS-GOA ($0.36563/kWh) is 80% lower than the electricity price of the conventional D_{GEN} system, which is found to be $1.81/kWh. Therefore, it can be concluded that the devised microgrid is competitive to standalone D_{GEN} currently used in most microgrid communities. Thus, this makes the project in the proposed case study area economically viable. It is also expected that the microgrid project if properly deployed will reduce greenhouse gasses, improve energy supply efficiency, and contribute to the constituency sustainable development goals objective.

Computation of the microgrid payback duration

To confirm the economic viability of the microgrid project, a detailed assessment of the project costs and revenue (free cash flow) is performed to determine the dynamic payback period. The analysis is carried out on the basis of the results obtained by the CEMS-GOA, as it showed the highest efficiency among the MOSTs analysed.

The dynamic payback period criterion integrates the concepts of the discounted cash flow analysis and static payback period method to determine the date at which the project becomes profitable on the basis of the discount rate. This technique was proposed for the first time by [47]. The criterion can, therefore, be applied in the field of microgrid sizing problem as follows:

$$\sum_{t=0}^{DPP} S(1+ir)^{-t} - NPC = 0 \tag{16}$$

where S denote the annual income generated by selling of electricity to the consumer. In this study, the COE value ($0.36563) as determined by the CEMS-GOA is used for the analysis. The S can be determined using Eq. (17).

$$S = 0.36563 \times P_{l,cum} \tag{17}$$

where $P_{l,cum}$ is the total annual supplied electrical loads (kW). The graphical discounted break-point of the planned microgrid on a revenue flow of 25years is shown in Fig. 16. As shown in the plot,

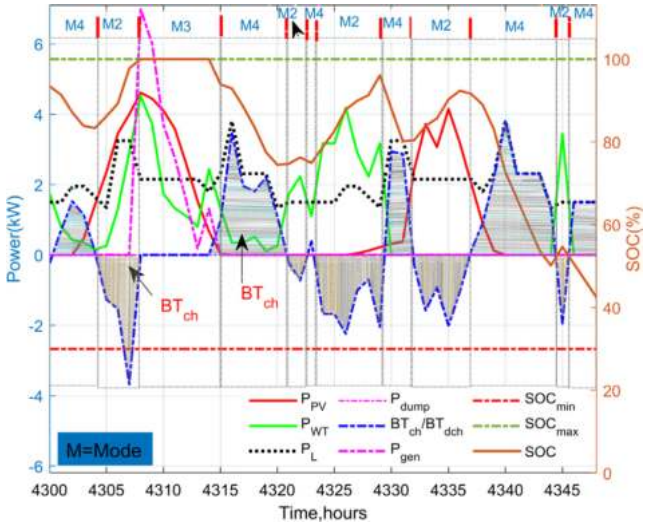

FIG. 11

Plot of electricity generation mix against the BT bank (Rainy-season).

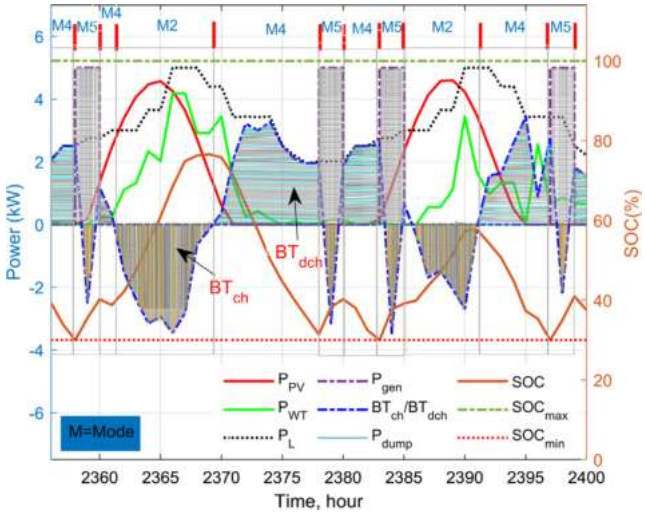

FIG. 12

Plot of electricity generation mix against the BT bank (Hot-season).

TABLE 2

Hour-by-hour execution of the REMS for 48 hours of operation in the cold weather.

Time, hour	Operating Conditions	Operating Modes	Consequence
1-9	$P_{PV} + P_{WT} < P_l$	Mode 4	P_{PV} , P_{WT} and BT bank supplying demand
9-18	$P_{PV} + P_{WT} > P_l$	Mode 2	P_{PV} , P_{WT} supplying demand and BT Charging
18-19	$P_{PV} + P_{WT} > P_l$	Mode 1	P_{PV} and P_{WT} supplying demand
19-33	$P_{PV} + P_{WT} < P_l$	Mode 4	P_{PV} , P_{WT} and BT bank supplying demand
33-41	$P_{PV} + P_{WT} > P_l$	Mode 2	P_{PV} , P_{WT} supplying demand and BT Charging
41-48	$P_{PV} + P_{WT} < P_l$	Mode 4	P_{PV} , P_{WT} and BT bank supplying demand

TABLE 3

Hour-by-hour execution of the REMS for 48 hours of operation in the rainy weather.

Time, hour	Operating Conditions	Operating Modes	Consequence
4300-4304	$P_{PV} + P_{WT} < P_l$	Mode 4	P_{PV} , P_{WT} and BT bank supplying demand
4304-408	$P_{PV} + P_{WT} > P_l$	Mode 2	P_{PV}, P_{WT} supplying demand and BT Charging
4308-4315	$P_{PV} + P_{WT} > P_l$	Mode 3	P_{PV} and P_{WT} supply demand and dump load
4315-4321	$P_{PV} + P_{WT} < P_l$	Mode 4	P_{PV} , P_{WT} and BT bank supplying demand
4321-4322	$P_{PV} + P_{WT} > P_l$	Mode 2	P_{PV}, P_{WT} supplying demand and BT Charging
4322-4323	$P_{PV} + P_{WT} < P_l$	Mode 4	P_{PV} , P_{WT} and BT bank supplying demand
4323-4329	$P_{PV} + P_{WT} > P_l$	Mode 2	P_{PV}, P_{WT} supplying demand and BT Charging
4329-4332	$P_{PV} + P_{WT} < P_l$	Mode 4	P_{PV} , P_{WT} and BT bank supplying demand
4332-4337	$P_{PV} + P_{WT} > P_l$	Mode 2	P_{PV}, P_{WT} supplying demand and BT Charging
4337-4344	$P_{PV} + P_{WT} < P_l$	Mode 4	P_{PV} , P_{WT} and BT bank supplying demand
4344-4346	$P_{PV} + P_{WT} > P_l$	Mode 2	P_{PV}, P_{WT} supplying demand and BT Charging

if implemented, the microgrid project's discounted payback period would be 11 years. Moreover, the discounted net income that can be made by selling electricity over the operational time-frame is estimated to be $54,129.6614. The linearity of the revenue curve shown in Fig. 16, is as a result of the simplistic assumption that the P_l is constant throughout the microgrid. Also, the non-linearity of the annualized cost curve is due to the cost associated with the replacement of the microgrid elements, whose lifespans are over, as well as the O&M cost. To determine the total cumulative annualized costs, the gross annualized capital expense is first determined, and then the adjusted O&M costs and replacement costs are added to the time which they incurred.

Also, note that after the microgrid operational time-frame (25year), the total annualized costs are equivalent to the best TNPC the CEMS-GOA has estimated ($135,899.6216). The break-even analysis shows that the microgrid investment is not only economically attractive but also offers a low-risk investment opportunity as a result of a short payback period.

Energy flow analyses

This section highlights the energetic assessments of the microgrid according to the optimum combination of microgrid elements estimated by the CEMS-GOA, whose dominance over other investigated MOSTs has been confirmed in the preceding section. This energetic assessment is performed on the basis of the best-case performance of the CEMS-GOA and the microgrid energy flow study is based on running the program simulating the CEMS-GOA for a period of one-year.

Figs. 17a, 17b, and 17c depict the plot P_{PV}, P_{WT}, P_{GEN} (the D_{GEN} power generation in the CEMS control strategy and it implies to the switch ON/OFF operation of the D_{GEN}) against the P_{GEN} in a standalone D_{GEN} for a year-long operation. Accordingly, the electricity generation mix of the microgrid is also portrayed in Fig. 17d. Note that, this study can be extended for the whole project lifespan. However, during the analysis, the sizes of the microgrid elements determined by the proposed capacity planning method should not be ignored. This will, therefore, prevent the discrepancies between the supply and demand imposed on the microgrid. The percentage contribution of the P_{PV}, BT, D_{GEN}, and P_{WT} to electricity generated by the microgrid is presented in Fig. 18. From the figure, it can be observed that 44% of the power generation from the microgrid is contributed by the PV array. The $D_{GEN,}$ BT bank, and WT have a share of 14%, 16%, and 26% of the total energy generated. The total annual energy harnessed from the PV array is 14,041kW/year. While, a total of 4343.5 kW/year, and 5154.4 kW/year is achieved from the WT and D_{GEN}, respectively.

In respect of the operation of the D_{GEN} which serves as a secondary backup supply (refer to Fig. 17c), it operates mostly during the hot season. This is due to the higher energy demand and perhaps, the BT bank is not allowed to be fully charged. The total operating hours of the D_{GEN} is 672 h per annum. With 50 h operating time dedicated to cold-season, while 470 h and

TABLE 4

Hour-by-hour execution of the REMS for 48 hours of operation in the hot weather.

Time, hour	Operating Conditions	Operating Modes	Consequence
2356-2358	$P_{PV} + P_{WT} < P_l$	Mode 4	P_{PV} , P_{WT} and BT bank supplying demand
2358-2360	$P_{PV} + P_{WT} < P_l$	Mode 5	D_{gen} supplying demand and BT Charging
2360-2361	$P_{PV} + P_{WT} < P_l$	Mode 4	P_{PV} , P_{WT} and BT bank supplying demand
2361-2369	$P_{PV} + P_{WT} > P_l$	Mode 2	P_{PV} , P_{WT} supplying demand and BT Charging
2369-2378	$P_{PV} + P_{WT} < P_l$	Mode 4	P_{PV} , P_{WT} supplying demand and BT Charging
2378-2380	$P_{PV} + P_{WT} < P_l$	Mode 5	D_{gen} supplying demand and BT Charging
2380-2383	$P_{PV} + P_{WT} < P_l$	Mode 4	P_{PV} , P_{WT} supplying demand and BT Charging
2383-2385	$P_{PV} + P_{WT} < P_l$	Mode 5	D_{gen} supplying demand and BT Charging
2385-2391	$P_{PV} + P_{WT} < P_l$	Mode 2	P_{PV} , P_{WT} supplying demand and BT Charging
2391-2397	$P_{PV} + P_{WT} < P_l$	Mode 4	P_{PV} , P_{WT} supplying demand and BT Charging
2397-2399	$P_{PV} + P_{WT} < P_l$	Mode 5	D_{gen} supplying demand and BT Charging

TABLE 5

Parameters settings for the MOSTs understudy.

MOSTs	Settings	Reference (s)
PSO	$w = 0.7, C_1 = 2, C_2 = 2$	[33]
ALO	Parameters are tuned adaptively (dynamic tuning)	[32]
CSA	$P_a = 0.2, P_c = 0.5$	[48]
GOA	$f = 0.5, l = 1.5$	[30]
GWO	Parameters are tuned adaptively (dynamic tuning)	[27]
DFA	$a = 0.1, w = 0.7, f = 1, s = 0.1, c = 0.7, e = 1$	[28]
SSA	Parameters are tuned adaptively (dynamic tuning)	[31]

152 h of operation are dedicated to the hot and rainy seasons, respectively. Analysis have also been conducted regarding the CO_2 emission, fuel consumption and COE of the proposed microgrid (scenario 1) and that of a standalone D_{GEN} (scenario 2). The result of the comparison is depicted in Fig. 19. The study indicates that the devised microgrid has considerably minimized the CO_2 and fuel consumption of D_{GEN} by 92.3%, 92.4%, and 79.8%, respectively.

On the other hand, the monthly projected P_{PV} and P_{WT} for the optimum capacity from January to December is portrayed in Figs. 20. The result shows that the P_{PV} trend is similar during the cold and hot season. The PV and WT generate the highest total power, of approximately 1243 kWh/month and 564 kWh/-month, respectively in the month of March. With a minimum P_{PV} of 34 kWh/day on the 2nd day and minimum P_{WT} of 1.1 kWh/day on the 5th day, respectively. The month of May has the second-highest power generation of 1225 kWh/month from the PV array, with a minimum generation of 24 kWh/day on the 10th day. For the WT the month of February, has the second power generation, of 467 kWh/month, with a minimum generation of 0.24 kWh/day. The minimum total power generation of 1033 kWh/month and 255 kWh/month is realized from the PV arrays and WT in August, with minimum power generation of 9.3 kWh/day and 0.15 kWh/day on the 6th and 24th day. The minimum power generated by the PV on the 6th day of August is also the minimum power generation in the year 2017, and this could be as a result of the rainy season in the month.

Furthermore, based on the hourly BT bank SOC exhibited in Fig. 21, it is shown that the SOC of the BT bank is more than 50% for about 49% hours in a year. The BT bank is drained to its minimum DoD (30%) for only 27 h in a year, and mostly in the hot season, to cope with energy demand. The subfigures shown in Figs. 21a and 21b present the analysis of the BT bank drain on the 1st day of January and the 2nd day of March. It can be noticed in Fig. 21a, at 0 h the BT bank began to drain from an initial SOC of 80% (equivalent 34 kWh) up to 8 h. Afterward, at 8 h the SOC starts to increase gradually during the charging process until it becomes fully charged at 14h.

Furthermore, during the period of operation of the microgrid, the excess power generated by the microgrid which can be channeled to the dump load, has been examined. The excess power results from microgrid when the demand cannot absorb the energy generated or when the maximum SOC of the BT is reached. Figs. 22 and 23 show the plot of the annual excess power generated and the share of the excess power for the different seasons. The analysis indicates that out of the 981.4 kW excess power generated, 17% (171.5 kW) of the share is generated during the rainy season, 1% (12.5 kW) in the hot season and 82% (811.3 kW) are generated in the cold season. The hot season is characterized by less excess power. This is because the

TABLE 6

Statistical analysis of the MOSTs in the minimization the COE

Metrics	CEMS-GWO	CEMS-ALO	CEMS-CSA	CEMS-DFA	CEMS-GOA	CEMS-SSA	CEMS-PSO
Best	0.367032	0.369835	0.366331	0.366331	0.365629	0.367522	0.367396
Worst	0.378441	0.389661	0.375567	0.387803	0.372358	0.381004	0.378679
Median	0.367032	0.369835	0.366331	0.366331	0.365629	0.367522	0.367396
Mean	0.368437	0.376569	0.367094	0.374257	0.366994	0.368877	0.368610
Avg	0.370235	0.376475	0.368831	0.373681	0.367653	0.371231	0.370520
Rank	3	7	2	6	1	5	4

TABLE 7

Analysis of the best COE achieved by the MOSTs out of 30 independent simulation run.

MOSTs	N_{PV}	PV array (kW)	N_{WT}	WT (kW)	BT bank capacity (kWh)	D_{GEN}(kW)	COE ($)	DPSP (%)	Total capital cost ($)	TNPC
CEMS-GWO	30.1	8,264	6.9	6,861	45.2	5	0.367032	0	60,976	140,119.5000
CEMS-ALO	32.8	9,023	7.8	7,681	45.2	5	0.369835	0	65,089	144,232.0000
CEMS-CSA	29.2	8,030	6.6	6,560	45.2	5	0.366331	0	57,802	138,745.4900
CEMS-DFA	32.5	8,940	7.3	7,320	45.2	5	0.366331	0	63,838	142,980.8923
CEMS-GOA	26.0	7,154	4.2	4,200	45.2	5	0.365629	0	50,029	135,899.6216
CEMS-SSA	32.0	8,788	7.2	7,150	45.2	5	0.367522	0	63,001	142,144.2266
CEMS-PSO	30.6	8,416	7.0	7,050	45.2	5	0.367396	0	61,901	141,044.2654

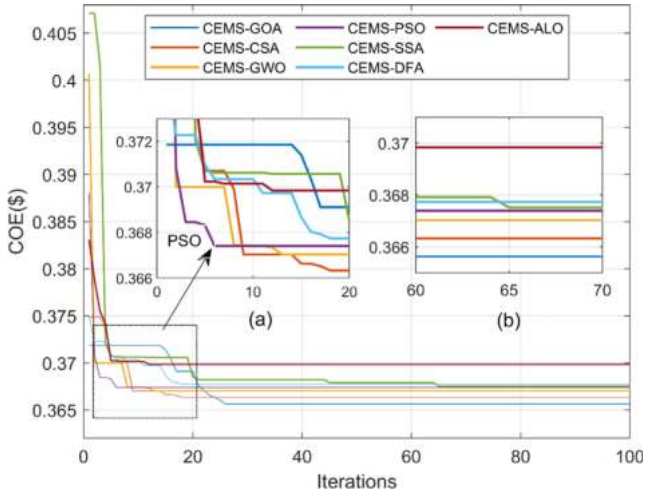

FIG. 13

The convergence plot of the best-case behaviours of the MOSTs over 30 cycles.

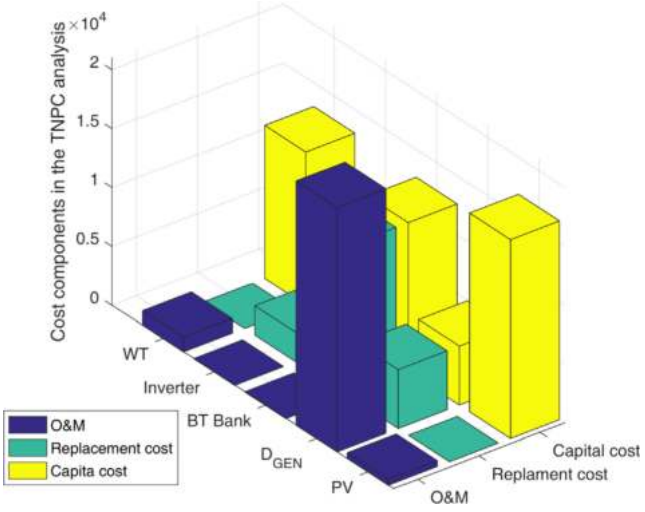

FIG. 15

Breakdown of the cash flow categories of the microgrid elements.

BT bank is extremely exploited during the season and particularly, the energy demand is high during the season.

Conclusions

This paper has presented MOSTs-based approach for the optimal design of an autonomous microgrid while trying to emphasize

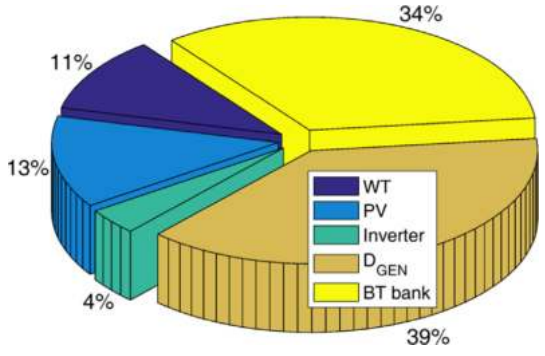

FIG. 14

Breakdown of the best TNPC calculated using CEMS-GOA out of 30 simulation runs.

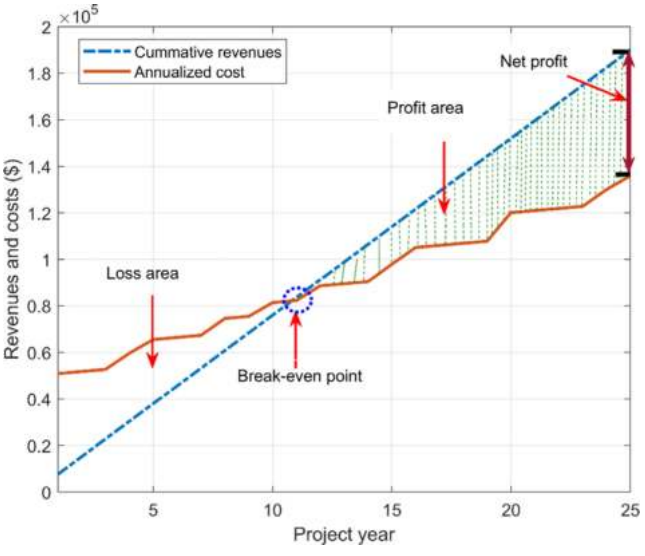

FIG. 16

The microgrid project break-even analysis over 25-years of service.

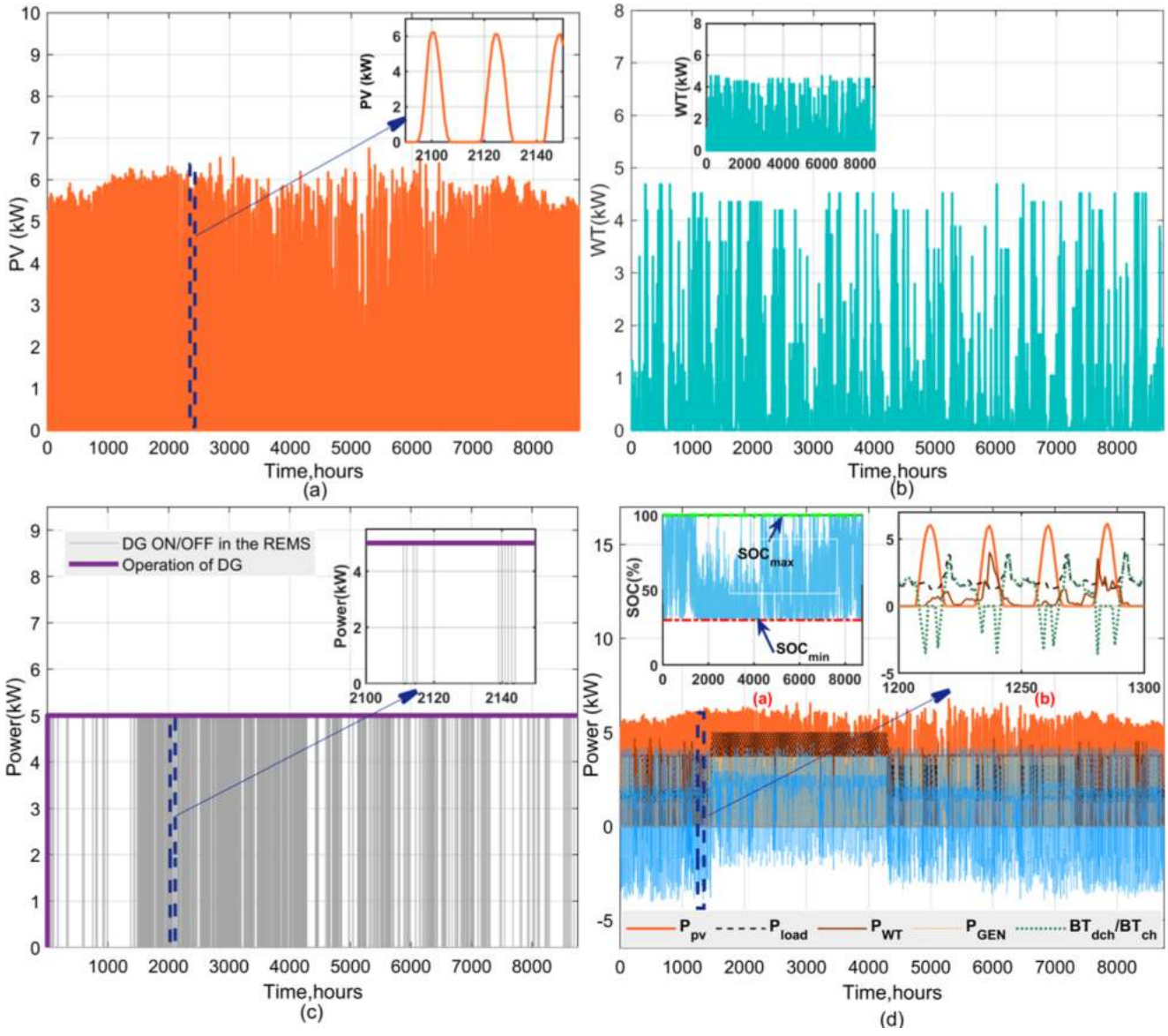

FIG. 17

(a) Plot of the P_{PV} (b) plot of the P_{WT} (c) plot the D_{GEN} power (P_{GEN}) (in the CEMS control strategy) against P_{GEN} in a standalone D_{GEN} (d) the annual electricity mix.

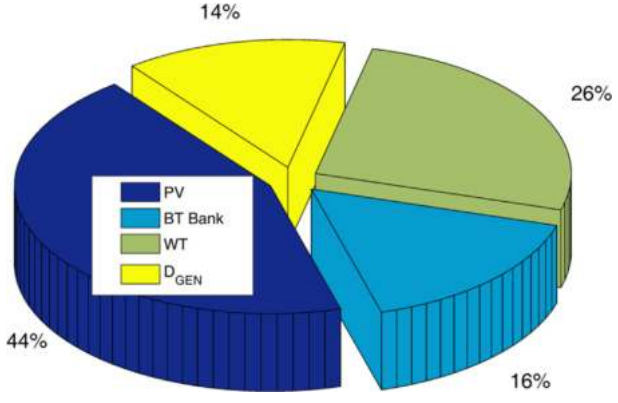

FIG. 18

The contribution of the PV, WT, DGEN, and BT to the total energy generation in the microgrid.

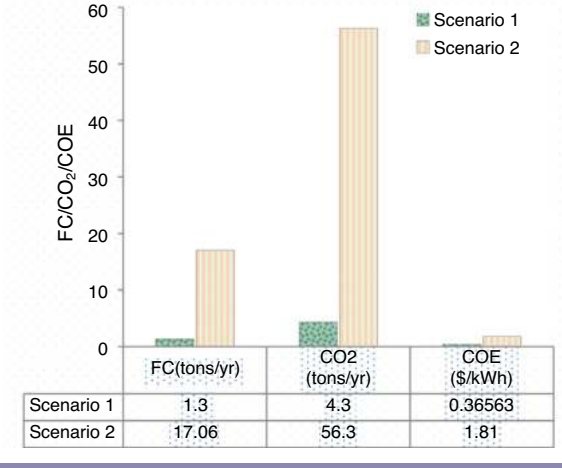

	FC(tons/yr)	CO2 (tons/yr)	COE ($/kWh)
Scenario 1	1.3	4.3	0.36563
Scenario 2	17.06	56.3	1.81

FIG. 19

Comparative analysis of scenario 1 and scenario 2 based on CO_2, FC, COE.

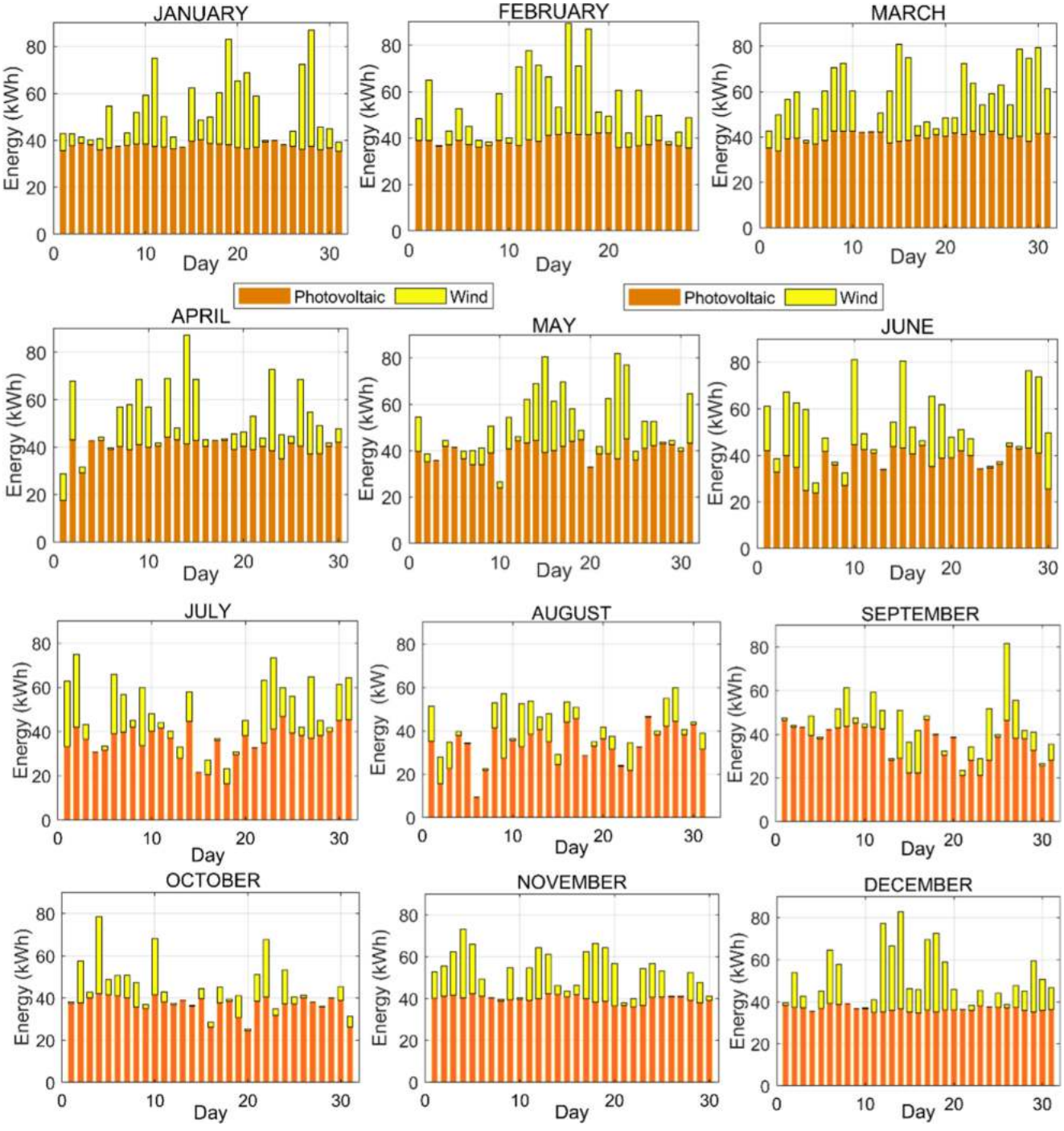

FIG. 20

Daily power generation by WT and PV for the month of January and December.

the importance of investigating newly developed MOSTs for microgrid capacity planning problem. Consequently, the outcomes of six MOSTs are compared with a well-document MOST in the research area (*i.e.,* PSO). Moreover, a statistical framework is devised for comparing of the examined MOSTs, taking into account the number of hits to the global optimum during the trials. A conceptual autonomous microgrid test-case system, devised to provide affordable electricity supply to residences of an isolated region in Yobe State, Nigeria, is selected as a study area for evaluating the output of MOSTs, and the comparative findings obtained are presented. The suggested RE-based microgrid offers a holistic framework for speeding up usage of RE systems and also increasing energy supply stability to remote regions which is in line with objective seven (GOAL 7: Clean and affordable energy) of the sustainable development goal.

The simulation results indicate that the CEMS-GOA method has outperformed the CEMS-PSO, CEMS-ALO, CEMS-SSA, CEMS-GWO, CEMS-CSA, and CEMS-DFA for the microgrid

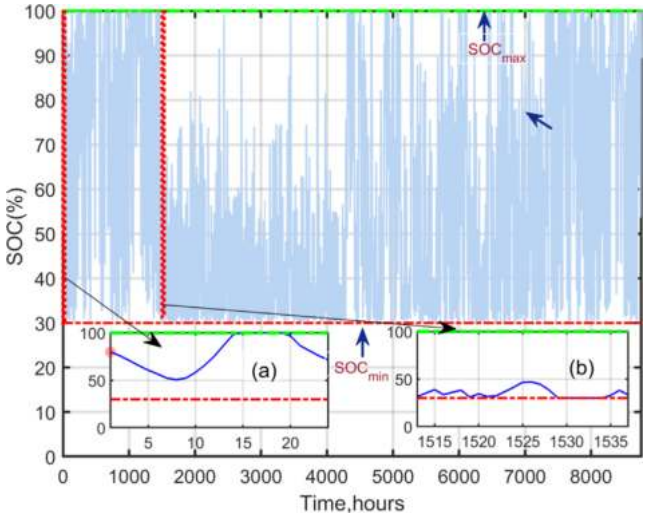

FIG. 21

One year-round available BT bank SOC (a) 1st day in January (b) 2nd day in March.

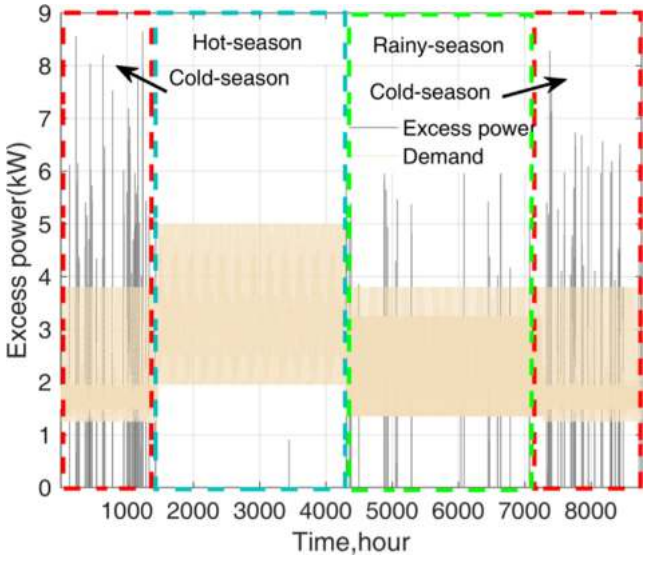

FIG. 22

Seasonal excess power generated against energy demand.

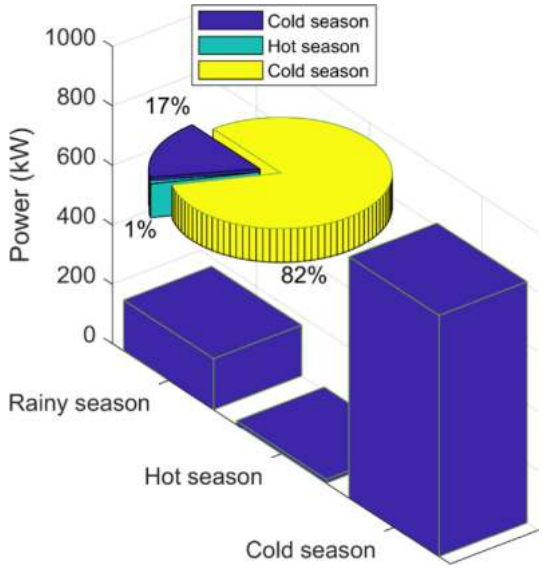

FIG. 23

The proportion of seasonal excess power generated.

design problem in terms quality of the solution set. However, the resilient exploitation capability of the GOA in the last iterations count decelerates its convergence pace, and this is not a serious issue since the problem at hand belongs to long-term energy planning infrastructure horizon, which implies that long-term simulation run times are acceptable in much as the numerical tractability is maintained. The exploitation capability exhibited by the CEMS-GOA method in the last iteration can be considered as its advantage in this research viewpoint. The results have also indicated that the CEMS adopted for the operational strategy of the microgrid has helped to better adoption of clean energy system since the strategy has significantly minimized the CO_2 (by 92.3%) and fuel consumption (by 92.4%), compared fossil fuel-based D_{GEN}. The discounted break-even analysis has also indicated the economic profitability of the microgrid project and low-risk investment opportunity because of the low payback period of 11 years if the project is executed.

Limitations and future prospects

This study has two drawbacks. One is that the study investigates only a small portion of the newly introduced MOSTs for the design of the autonomous microgrid problem. Second, the efficiency of the MOSTs is investigated on a single microgrid system configuration.

To realize the foregoing drawbacks, new MOSTs should be employed for the microgrid planning problem. In addition, the efficiency of the MOSTs should be investigated on a complex system, such as microgrid pool (interconnection of two or more microgrids). Another trend for future research is to create a podium to examine the harmonics emanating from the converters linking the various energy sources and the loads to the microgrid common bus when designing the microgrid.

Declaration of Competing Interest

The authors declare that they have no known competing financial interests or personal relationships that could have appeared to influence the work reported in this paper.

Acknowledgement

The authors would like to thank and acknowledged funding provided by UTMshine under vote Q.J130000.2451.09G32.

References

[1] T. Castillo-Calzadilla et al., J. Cleaner Prod. 244 (2020) 118870.
[2] P. Kumar, N. Pal, H. Sharma, J. Storage Mater. 41 (2021) 102965.
[3] P. Cortés et al., J. Cleaner Prod. 252 (2020) 119772.
[4] D.T. Ton, M.A. Smith, Electric. J. 25 (8) (2012) 84–94.
[5] A.L. Bukar, C.W. Tan, J. Cleaner Prod. (2019).
[6] S. Ahmadi, S. Abdi, Sol. Energy 134 (2016) 366–374.
[7] G. Ma et al., IET Renew. Power Gener. 11 (1) (2016) 194–202.
[8] A.K. Bansal, R. Kumar, R. Gupta, IEEE Trans. Smart Grid 4 (1) (2013) 638–648.
[9] C. Gamarra, J.M. Guerrero, Renew. Sustain. Energy Rev. 48 (2015) 413–424.

[10] X.-S. Yang, Nature-inspired mateheuristic algorithms: Success and new challenges. arXiv preprint arXiv:1211.6658, 2012.
[11] A.L. Bukar et al., Int. J. Power Electron. Drive Syst. 11 (3) (2020) 1527–1535.
[12] S. Mohseni, A.C. Brent, Int. J. Hydrogen Energy (2019).
[13] M.D.A. Al-falahi, S.D.G. Jayasinghe, H. Enshaei, Energy Convers. Manage. 143 (2017) 252–274.
[14] A.S. Lopes, R. Castro, C. Silva, J. Storage Mater. 18 (2018) 196–205.
[15] A. Maleki, M.A. Nazari, F. Pourfayaz, Energy Rep. (2020).
[16] B. Li et al., Appl. Energy 205 (2017) 1244–1259.
[17] S. Mohseni, A.C. Brent, D. Burmester, Energy Convers. Manage. 200 (2019) 112105.
[18] M. Jahannoosh, S.A. Nowdeh, Appl. Soft Comput. (2020) 106611.
[19] A. Fathy, K. Kaaniche, T.M. Alanazi, IEEE Access 8 (2020) 57630–57645.
[20] H. Nasiraghdam, S. Jadid, Sol. Energy 86 (10) (2012) 3057–3071.
[21] A. Chauhan, R. Saini, Renew. Energy 94 (2016) 587–604.
[22] N. Mohandas, R. Balamurugan, L. Lakshminarasimman, Int. J. Electr. Power Energy Syst. 66 (2015) 41–52.
[23] M. Jahannoosh et al., J. Cleaner Prod. (2020) 123406.
[24] Y. Jiao et al., Discr. Dyn. Nature Soc. 2017 (2017).
[25] G. Derakhshan, H.A. Shayanfar, A. Kazemi, Int. J. Hydrogen Energy 41 (44) (2016) 19947–19956.
[26] T. Tezer, R. Yaman, G. Yaman, Renew. Sustain. Energy Rev. 73 (2017) 840–853.
[27] S. Mirjalili, S.M. Mirjalili, A. Lewis, Adv. Eng. Softw. 69 (2014) 46–61.
[28] S. Mirjalili, Neural Comput. Appl. 27 (4) (2016) 1053–1073.
[29] X.-S. Yang, Nature-inspired metaheuristic algorithms, Luniver Press, 2010.
[30] S. Saremi, S. Mirjalili, A. Lewis, Adv. Eng. Softw. 105 (2017) 30–47.
[31] S. Mirjalili et al., Adv. Eng. Softw. 114 (2017) 163–191.
[32] S. Mirjalili, Adv. Eng. Softw. 83 (2015) 80–98.
[33] J. Kennedy, R. Eberhart, Particle swarm optimization, Proceedings of ICNN'95-international conference on neural networks, IEEE, 1995.
[34] N. Ghorbani et al., Energy 154 (2018) 581–591.
[35] O. Nadjemi et al., Renew. Sustain. Energy Rev. 70 (2017) 1352–1365.
[36] J. Bandopadhyay, P.K. Roy, Appl. Soft Comput. (2020) 106487.
[37] A.R. Bhatti, Z. Salam, Renew. Energy 125 (2018) 384–400.
[38] H. Borhanazad et al., Renew. Energy 71 (2014) 295–306.
[39] M.F. Zia, E. Elbouchikhi, M. Benbouzid, Appl. Energy (2018).
[40] F.E.-Z. Lamzouri, E.-M. Boufounas, A. El Amrani, J. Storage Mater. 42 (2021) 103044.
[41] A.R. Bhatti et al., Renew. Sustain. Energy Rev. 54 (2016) 34–47.
[42] A.L. Bukar, C.W. Tan, L.K. Yiew, R. Ayop, W.S. Tan, Energy Convers. Manage. 221 (2020).
[43] N.M. Isa, et al., Optimal Sizing of Hybrid Fuel Cell and PV Employing Hybrid PSO-GA, in: 2019 IEEE Conference on Energy Conversion (CENCON), IEEE, 2019.
[44] Nigerian Meteorological Agency (NIMET). https://nimet.gov.ng/nwp Retrieved [accessed 04.18.2017].
[45] Central Bank of Nigeria (CBN). Current interest rate. https://www.cbn.gov.ng/ [accessed 08.10.2019].
[46] N. Veček, M. Črepinšek, M. Mernik, Appl. Soft Comput. 54 (2017) 23–45.
[47] X.-S. Yang, S. Deb, Cuckoo search via Lévy flights, in: 2009 World congress on nature & biologically inspired computing (NaBIC), IEEE, 2009.
[48] I. Fisher, Theory of interest: as determined by impatience to spend income and opportunity to invest it, Augustusm Kelly Publishers, Clifton, 1930.